Supplementary Information (SI) for Lab on a Chip.

Supplementary Information for Development of a 16-Channel Solid-State Nanopore Array Platform for Integrated Nanopore Fabrication and Ionic Current Measurement

Itaru Yanagi*[1], Tadashi Kiyuna*[2], Keiko Esashika*[3], Yoshimitsu Yanagawa*[4], Hai Huy Nguyen Pham*[4], Daiki Kawai*[1], Satoshi Ogihara*[1], Gaku Ogino*[1], Ken-ichi Takeda*[4] and Sotaro Uemura*[1]

[1]Department of Biological Sciences, Graduate School of Science, The University of Tokyo, Tokyo, 113-0033, Japan

[2]Hitachi Information & Telecommunication Engineering, Ltd, Yokohama, 220-6122, Japan

[3]Department of Electronics and Electrical Engineering, Keio University, Yokohama, 223-8522, Japan

[4]Healthcare Innovation Center, Research & Development Group, Hitachi, Ltd., Tokyo, 185-8603, Japan

The Supporting Information includes:

SI-1. Schematic illustrations of the assembled flow cell and photographs of the membrane chips

Figure S-1(a) presents a schematic illustration of the assembled flow cell, and (b) shows the configuration with the electrode array. (c) Photographs of the front and back sides of a membrane chip.

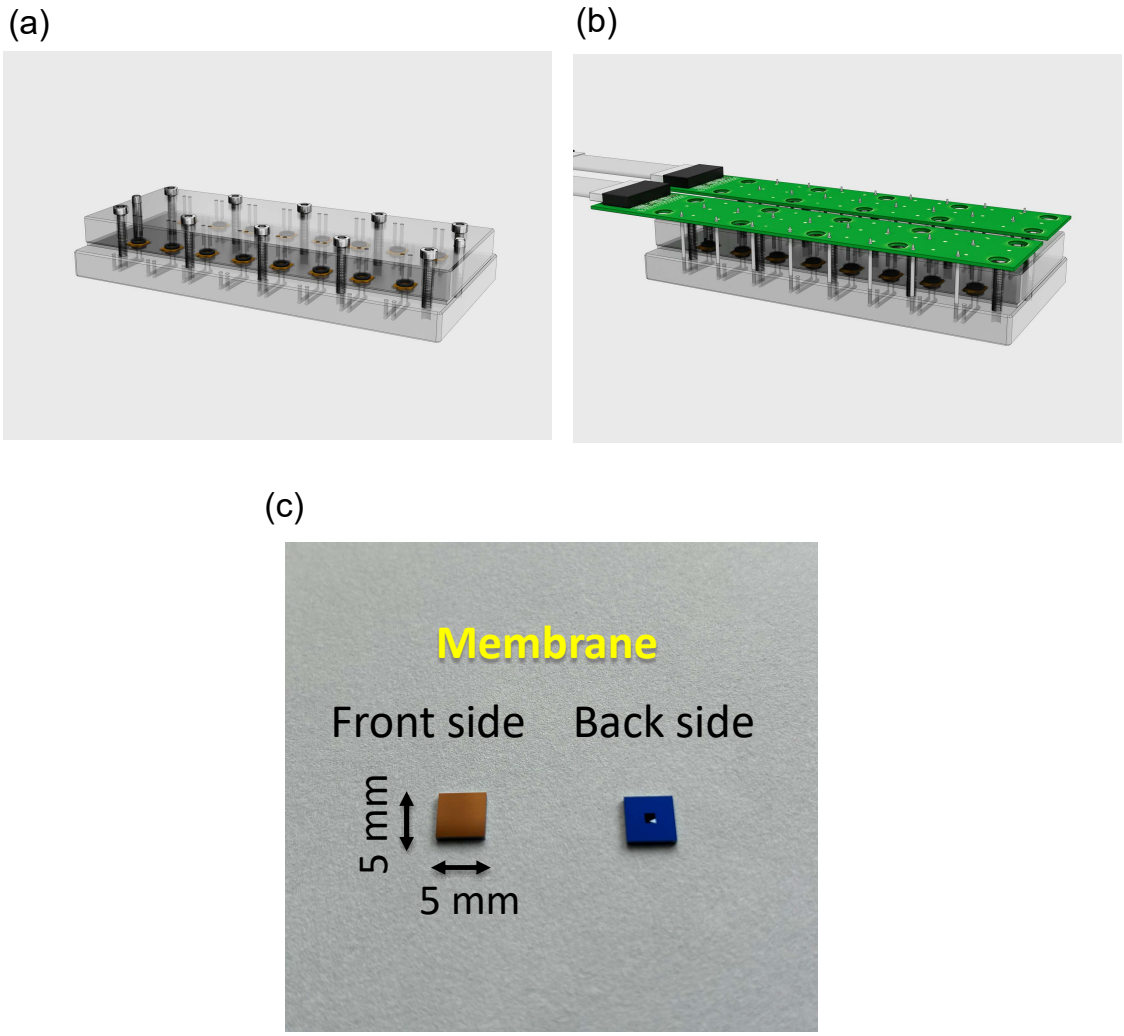

Figure S-1

SI-2. Representative screenshot of the control software

Figure S-2 presents a partial screenshot of the custom-developed control software. The screenshot was captured during the simultaneous measurement of DNA translocation events through 16 nanopores. On the right side of the screen, ionic current traces from all 16 channels are displayed. The lower panel shows a 1 s magnified view of the ionic current trace from a selected channel. The left panel displays the power spectrum of the current from the selected channel.

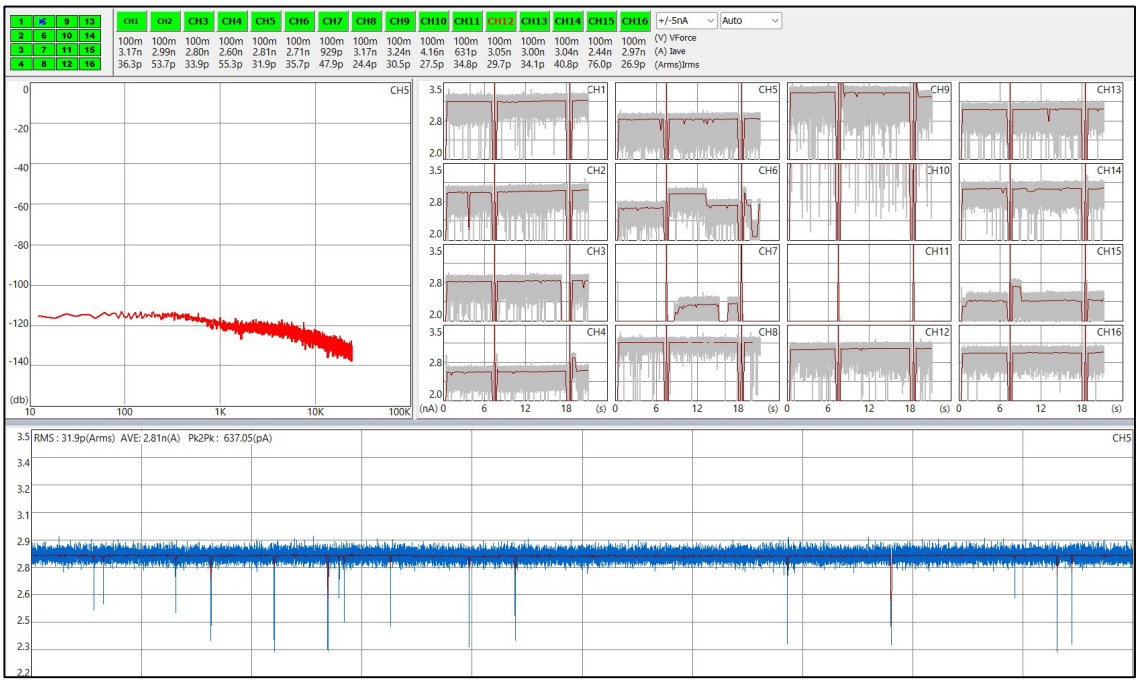

Figure S-2

SI-3. Details of the main components used in the circuit board

A list of the main components used in the circuit board of the 16-channel measurement system is provided below.

Table S-1

Function	Parts Name	Parts number	Supplier	Quantity
Communication	USB-IF	FT232HL	FTDI Chip	1
Controller	FPGA	EP2C5T144C8N	Altera	1
Sub controller	CPLD	5M160ZE64C5N	Altera	6
Voltage control	DAC	AD5754BREZ	Analog Devices	5
Isolation	Isolator	ISO7741DBQ	Texas Instruments	9
Analog sensing	ADC	ADS8598HIPM	Texas Instruments	2
Head amp.	OPAMP	OPA637AU	Texas Instruments	16
Pore fab.	Sub amp.	OPA2191IDGKR	Texas Instruments	36
Analog switch	Switch	ADG333ABRSZ	Analog Devices	32
Hi-res	res	CRHV1206AF1G00FKE5	Vishay Techno	17
Controller power	DC-DC	R1SE-0505-R	RECOM Power	1
LDO	LDO	TLV71333PDBVR	Texas instruments	1
LDO	LDO	TLV713185PDBVR	Texas instruments	1
+/- 12V	DC-DC	LT3471EDD#PBF	Linear Technology	3
Low noise LDO	LDO	TPS7A3001DRBT	Texas instruments	2
Low noise LDO	LDO	TPS7A4701RGWT	Texas Instruments	3

SI-4. Flowchart of the MPVI procedure

Figure S-3 shows flowcharts of the nanopore generation (a) and widening (b) processes using MPVI.

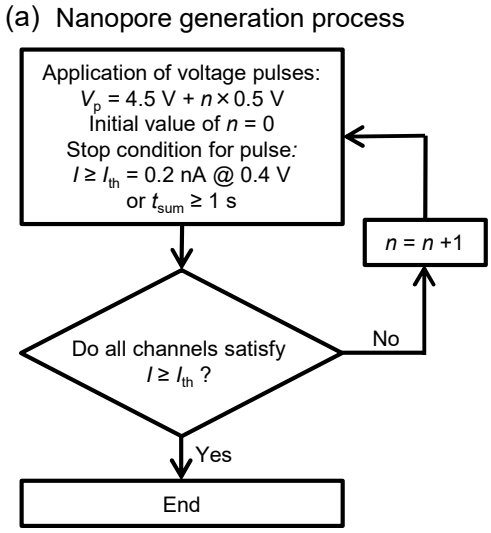

※Once $I \geq I_{th}$ is satisfied, voltage pulses are no longer applied to that channel.

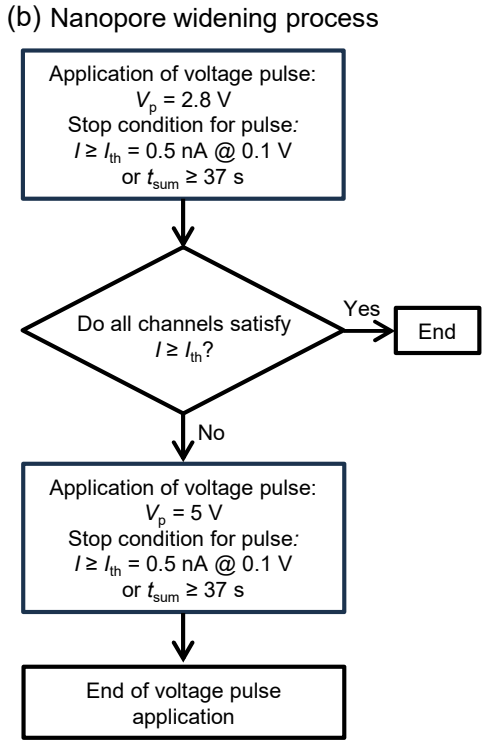

※Once $I \geq I_{th}$ is satisfied, voltage pulses are no longer applied to that channel.

Figure S-3

SI-5. Summary of nanopore diameters and poly(dT)$_{60}$ translocation characteristics for each channel

Table S-2 summarizes the nanopore diameters and poly(dT)$_{60}$ translocation characteristics for each channel. ΔI_P is defined as the highest peak of the smoothed ΔI histogram. Δt_D and ΔI_D are defined as the Δt and ΔI values corresponding to the highest-density point in each Δt–ΔI scatter plot.

Table S-2

Ch. #	Pore diameter (nm)	No. of events	Event frequency (/s)	ΔI_P (nA)	ΔI_D (nA)	Δt_D (ms)
1	1.14	5365	62.4	0.418	0.407	0.18
2	2.13	1603	12.4	0.533	0.660	0.12
3	1.00	2756	22.4	0.542	0.545	9.36
4	1.54	3206	19.2	0.737	0.708	0.24
5	1.76	365	3.2	0.551	0.552	0.12
6	1.39	2523	20.7	0.686	0.676	0.46
7	2.05	902	18.0	0.523	0.487	0.12
8	0.69	Too few events	N/A	N/A	N/A	N/A
9	0.48	Too few events	N/A	N/A	N/A	N/A
10	0.12	Too few events	N/A	N/A	N/A	N/A
11	1.35	Too few events	N/A	N/A	N/A	N/A
12	1.30	3316	21.1	0.628	0.623	1.38
13	0.89	Too few events	N/A	N/A	N/A	N/A
14	1.49	3090	34.7	0.690	0.681	0.24
15	2.05	1931	12.1	0.526	0.637	0.1
16	1.44	6349	39.7	0.727	0.726	1.26

SI-6. Relationships among pore diameter, ΔI_P, and ΔI_D for poly(dT)$_{60}$ translocation

Figure S-4(a) presents the dependence of ΔI_P on nanopore diameter (ϕ). The tendency for ΔI_P to reach a maximum near 1.5 nm is consistent with the ΔI_D versus ϕ trend shown in Fig. 6(b) of the main text. Figure S-4(b) presents the relationship between ΔI_P and ΔI_D. For most channels, ΔI_P and ΔI_D are in close agreement.

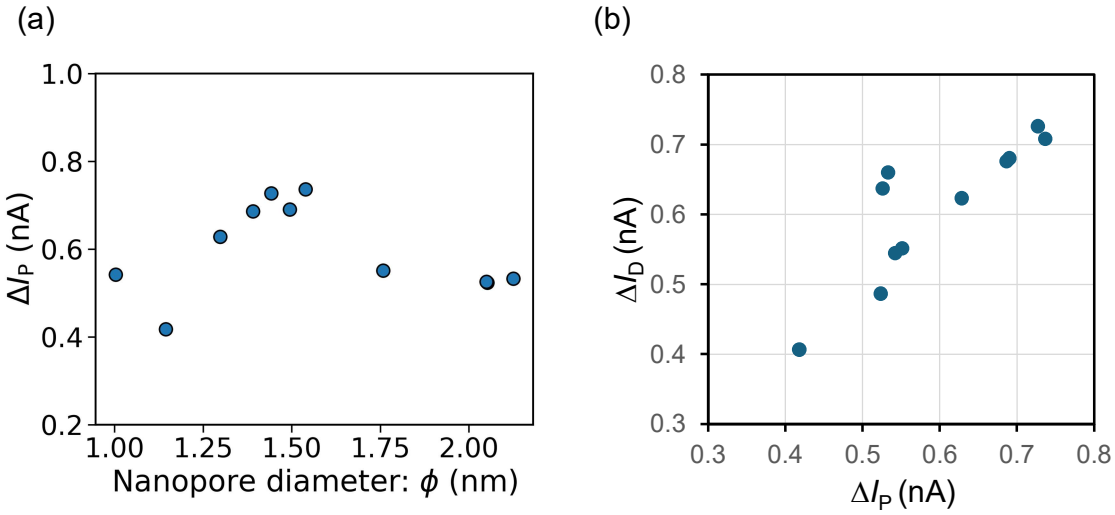

Figure S-4

SI-7. CBD characteristics of 20-nm-thick SiN membranes and distribution of the fabricated nanopore diameters

Figure S-5(a) shows the CBD characteristics of all 16 channels for nanopore fabrication in 20-nm-thick SiN membranes, from the dielectric breakdown point to the end-of-NP-fabrication point. The experiment was performed in KCl aqueous solution at pH 12.7 by applying -18 V to each *trans* chamber with the threshold current set to Ith = 600 nA. Figure S-5(b) shows the *I–V* characteristics of all 16 channels after CBD. Figure S-5(c) shows the estimated diameters of the fabricated nanopores, calculated from the current values at 0.1 V using eqn (1), presented as box-and-whisker plots together with those for the 14-nm-thick SiN membranes shown in Fig. 8 in the main text. Excluding outliers, the variation in the fabricated nanopore diameters is very small for both the 20-nm-thick and 14-nm-thick membranes, remaining within 2 nm.

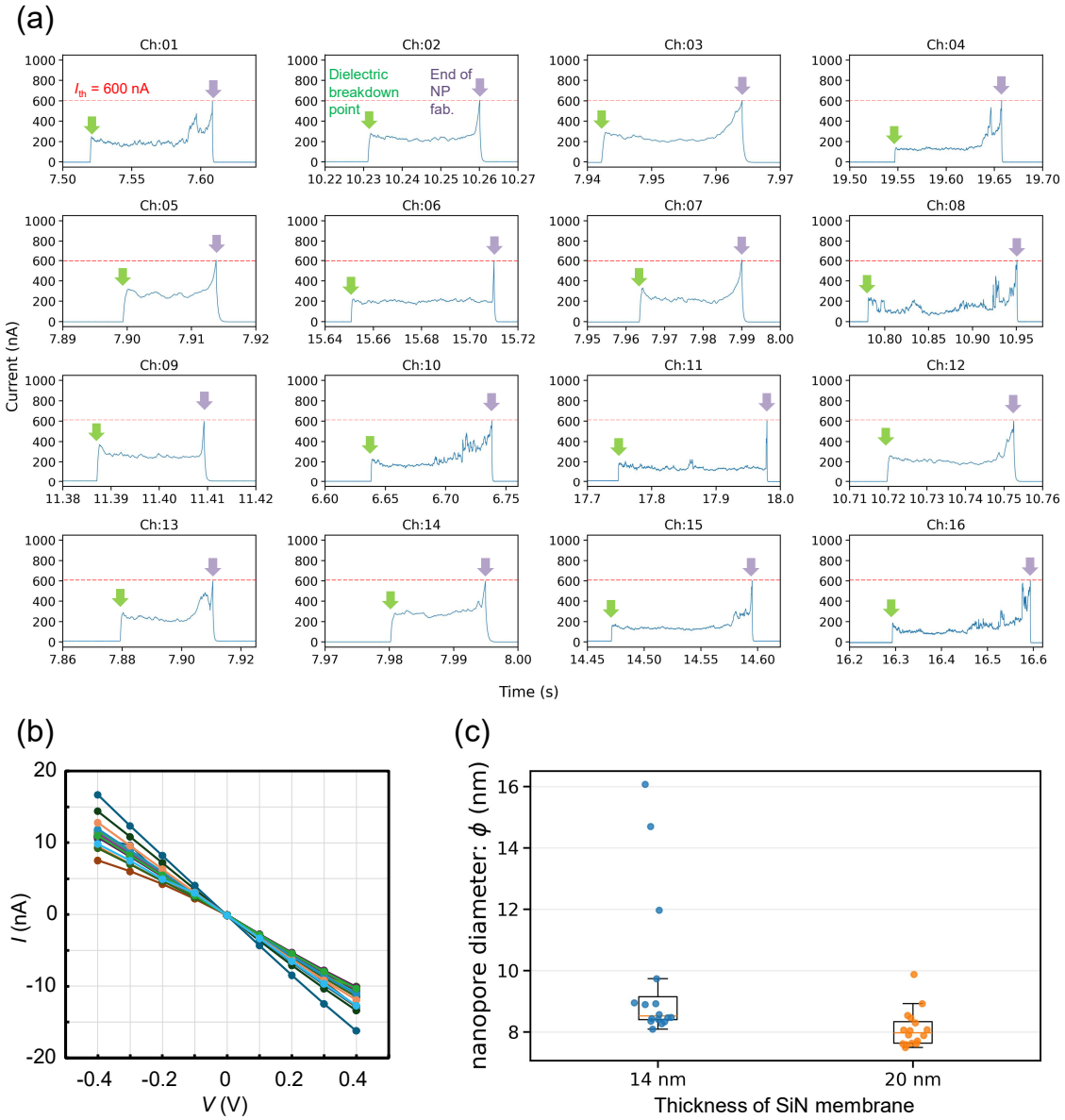
(a)
Ch:01
Ch:02
Ch:03
Ch:04
Ch:05
Ch:06
Ch:07
Ch:08
Ch:09
Ch:10
Ch:11
Ch:12
Ch:13
Ch:14
Ch:15
Ch:16
I_{th} = 600 nA
Dielectric breakdown point
End of NP fab.
Current (nA)
Time (s)
(b)
I (nA)
V (V)
(c)
nanopore diameter: ϕ (nm)
14 nm
20 nm
Thickness of SiN membrane

Figure S-5

SI-8. Summary of nanopore diameters and 400 bp dsDNA translocation characteristics for each channel

Table S-3 summarizes the nanopore diameters and 400 bp dsDNA translocation characteristics for each channel. ΔI_P is defined as the highest peak of the smoothed ΔI histogram. Δt_D and ΔI_D are defined as the Δt and ΔI values corresponding to the highest-density point in each Δt–ΔI scatter plot.

Table S-3

Ch. #	Pore diameter (nm)	No. of events	Event frequency (/s)	ΔI_P (nA)	ΔI_D (nA)	Δt_D (ms)
1	9.31	7560	29.65	0.597	0.565	0.14
2	10.69	1168	30.74	0.593	0.567	0.18
3	9.33	6128	23.21	0.568	0.491	0.14
4	13.87	9069	34.35	0.604	0.408	0.1
5	9.09	8690	32.92	0.637	0.599	0.18
6	9.34	5696	21.58	0.608	0.578	0.16
7	9.39	4196	15.89	0.556	0.478	0.14
8	9.81	2284	8.65	0.467	0.416	0.1
9	9.47	6506	24.64	0.563	0.473	0.14
10	18.84	6078	24.81	0.466	0.434	0.12
11	9.60	734	2.78	0.532	0.452	0.14
12	10.28	5507	81.89	0.466	0.443	0.12
13	10.83	2238	74.60	0.680	0.679	2.98
14	9.66	708	2.78	0.512	0.468	0.14
15	9.10	4497	17.64	0.743	0.707	0.14
16	16.28	4849	69.27	0.754	0.731	0.12

SI-9. Relationships among pore diameter, ΔI_P, and ΔI_D for 400 bp dsDNA translocation

Figure S-6(a) presents the dependence of ΔI_P on nanopore diameter (ϕ). The trend is similar to that shown in Fig. 11 of the main text, and no clear dependence on pore diameter is observed. Figure S-6(b) presents the relationship between ΔI_P and ΔI_D. For most channels, ΔI_P and ΔI_D are in close agreement.

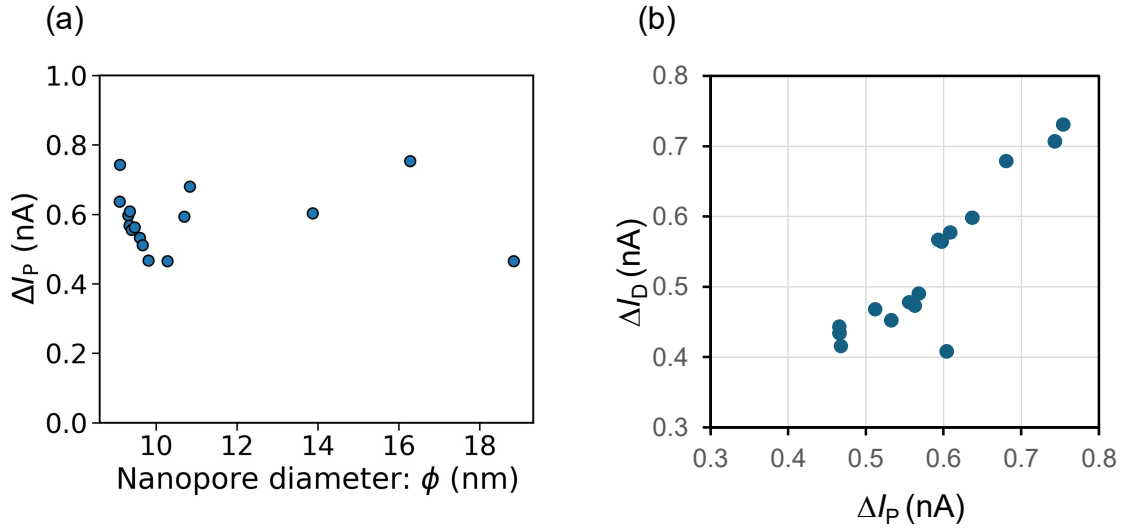

Figure S-6

SI-10. Noise characteristics of the baseline current through nanopore membranes

Figure S-7(a) shows a typical ionic current through a nanopore formed in a 5-nm-thick SiN membrane fabricated using the poly-Si sacrificial layer process, while Figure S-7(b) shows the ionic current through a nanopore formed in a 14-nm-thick SiN membrane fabricated using the SiO_2 sacrificial layer process. The nanopore diameters were 1.26 nm for (a) and 9.65 nm for (b). The aqueous solutions were 1 M KCl at pH 8.7 for (a) and 1 M KCl at pH 7.5 for (b), and the applied voltage was 0.1 V in both cases. Figure S-7(c) shows the noise power spectra for the two cases. As described in our previous report [1], membranes fabricated using the SiO_2 sacrificial layer process have lower capacitance than those fabricated using the poly-Si sacrificial layer process, resulting in lower noise.

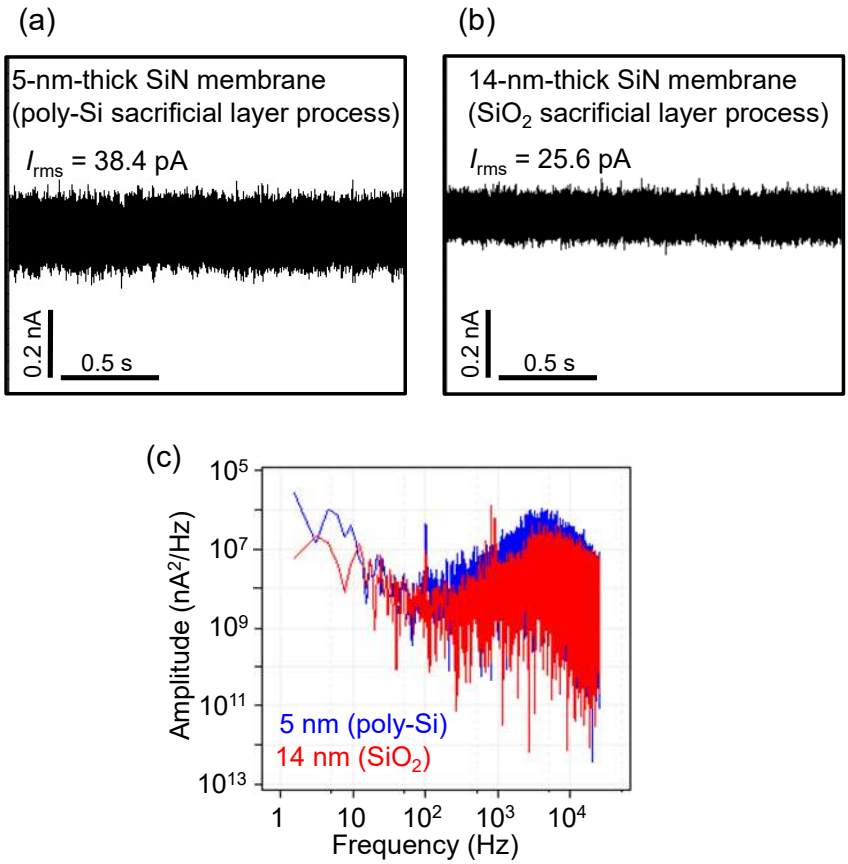

Figure S-7

SI-11. Open-input RMS current noise and RMS current noise with nanopores connected

Tables S-4(a) and S-4(b) show, respectively, the open-input RMS current noise and the RMS current noise with nanopores connected, both measured in the 16-channel measurement system. In each table, the values are listed for the case where all 16 channels were operated simultaneously (16 ch active) and for the case where only the individual channel under measurement was operated (1 ch active; the other 15 channels were disabled). It was confirmed that there were no large differences in RMS current noise among the channels, and that there was almost no difference in RMS current noise between the 16 ch active and 1 ch active conditions. The applied voltage was 0.1 V for both Tables S-4(a) and S-4(b). For the measurement in Table S-4(b), nanopores formed in 14-nm-thick SiN membranes were used, and the aqueous solution used was 1 M KCl at pH 8.7.

Table S-4 (a)

ch	Irms (pA) @ 16 ch active	Irms (pA) @ 1 ch active
1	3.43	3.38
2	1.94	2.15
3	2.4	2.87
4	2.09	2.58
5	3.05	3.1
6	2.36	2.67
7	2.22	2.57
8	2.68	2.54
9	2.28	3.05
10	3.07	3.1
11	2.21	2.37
12	2.32	2.75
13	3.26	3.22
14	3.02	3.08
15	3.39	3.68
16	3.4	3.46

Table S-4 (b)

ch	Irms (pA) @ 16 ch active	Irms (pA) @ 1 ch active	pore diameter (nm)
1	27.8	27.7	11.4
2	25.5	25.1	15.1
3	24.2	23.3	11.2
4	24.3	24	9.75
5	26.4	26.3	10.7
6	26.4	26.6	12.4
7	27.3	25.6	10.5
8	25.7	25.9	11
9	22.5	22.8	10.6
10	26.1	26.9	11.1
11	24	23.2	11.7
12	25.3	24.9	10.2
13	29.6	29.4	10.2
14	26.3	25.9	11.7
15	28.2	27.8	14.1
16	24.9	23.4	10.9

SI-12. Verification of crosstalk in blockade-current signals between adjacent channels

Figures S-8(a) and (b) show enlarged views of the current traces for ch5 and ch6, and for ch9 and ch10, respectively, from the measurements presented in Figure 9 of the main text, during periods in which a blockade current was observed in one of the two channels. As shown in the figures, when a blockade current was observed in one channel, no correlated fluctuation was observed in the adjacent channel, indicating the absence of inter-channel crosstalk in the blockade-current signal.

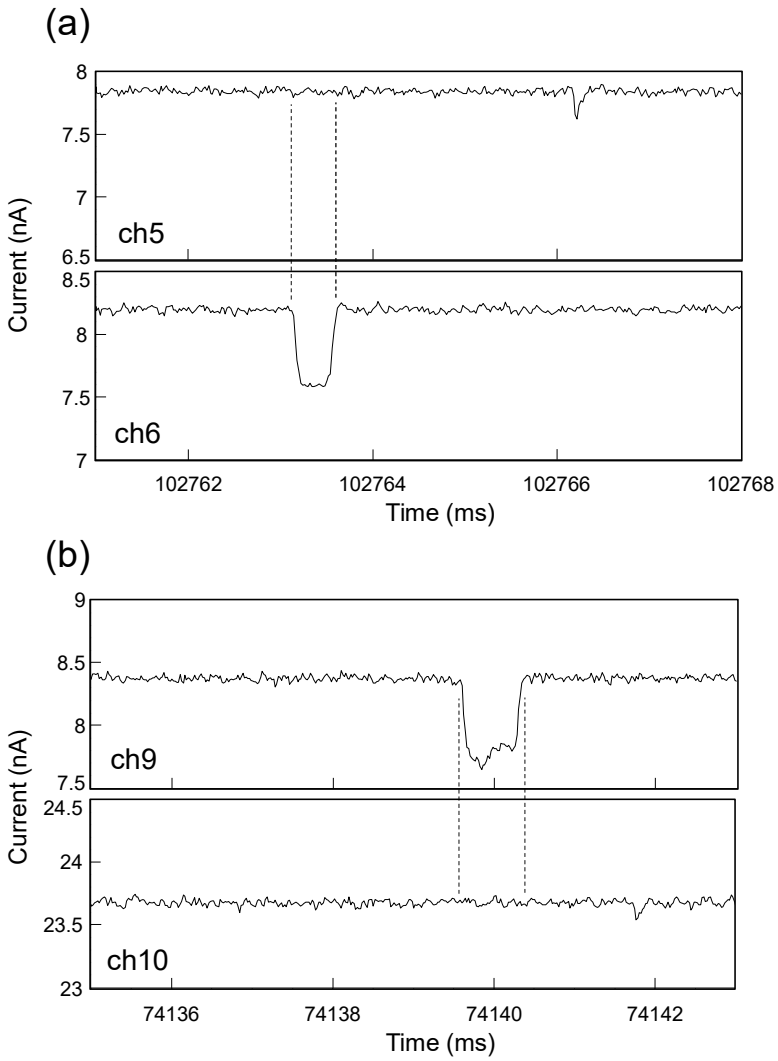

Figure S-8

References

[1] I. Yanagi and K. Takeda, *Nanotechnology*, 2021, 32, 415301.